

Electric field effect on electron spin splitting in SiGe/Si quantum wells

M.O. Nestoklon and E.L. Ivchenko

A.F. Ioffe Physico-Technical Institute, Russian Academy of Sciences, St. Petersburg 194021, Russia

J.-M. Jancu and P. Voisin

Laboratoire de Nanophotonique et Nanostructures, 91460 Marcoussis, France

Effect of electric field on spin splitting in SiGe quantum wells (QWs) has been studied theoretically. Microscopical calculations of valley and spin splittings are performed in the efficient $sp^3d^5s^*$ tight-binding model. In accordance with the symmetry considerations, the electric field not only modifies the interface induced spin splitting but gives rise to a Rashba-like contribution to the effective two-dimensional electron Hamiltonian. Both the valley and spin splittings oscillate as a function of the QW width due to inter-valley reflection of the electron wave off the interfaces. The oscillations of splitting are suppressed in rather low electric fields. The tight-binding calculations have been analyzed by using the generalized envelope function approximation extended to asymmetrical QWs.

PACS numbers: 73.21.Fg, 78.67.De

I. INTRODUCTION

Understanding the details of semiconductor heterostructure electronic properties has been a key at each stage of their applications in the field of information and communication technologies. Presently, there is a broad interest in spin-dependent properties because they have a potential for novel “spintronic” devices, and beyond, because they govern for a large part the possible development of semiconductor-based quantum information processing. Spin splitting of electron dispersion relations arises from the combination of spin-orbit coupling and inversion asymmetry. Besides the contributions of bulk inversion asymmetry (BIA) first discussed by Dresselhaus in 1954 and the structure inversion asymmetry (SIA) introduced by Rashba,^{1,2} the existence of a contribution due to the breakdown of roto-inversion symmetry at an interface between two semiconductors was first suggested by Vervoort et al. in the late 90s.^{3,4} This “interface inversion asymmetry” (IIA) term was further documented both by group-theoretical analysis,⁵ envelope-function calculations⁴ and measurements of circular polarization relaxation in quantum wells (QWs) based on various III-V semiconductors.^{6,7,8} However, in these cases, the interface contribution appears in combination with BIA and SIA. Pure IIA can exist alone or together with SIA in heterostructures of centro-symmetric semiconductors like Si-Ge QWs. Previous works⁹ have established the symmetry properties specific to this system where electrons lie in states originating from the bulk X_z valleys. A general feature of zone-edge conduction valleys in bulk materials is their degeneracy (6 for X -valleys, 4 for L -valleys) that gives rise to strong valley-coupling when they are folded onto the two-dimensional Brillouin zone of a QW.^{10,11,12,13,14,15} Valley coupling is another manifestation of the local, three-dimensional variations of crystal potential at semiconductor interfaces and quantitative estimates require atomistic information which is not available within the $\mathbf{k} \cdot \mathbf{p}$ theoret-

ical framework. Parameters describing valley coupling must be extracted from microscopic approaches such as ab-initio calculations or modelizations using empirical parametrizations like atomistic pseudopotentials or tight-binding approach. The valley coupling strongly depends on the crystalline growth direction and shows an oscillating behaviour as a function of the number of monolayers forming the X_z -valley or L -valley quantum well. It also depends on the overall symmetry of the quantum well and for this reason, it can be modified by an external electric field. The spin-splittings of in-plane dispersion relations in such systems results from the interplay of valley coupling and spin-dependent terms in the electron Hamiltonian. The case of L -valley QWs formed in the GaSb-AlSb system and grown along the $[001]$ direction was first discussed in some details by Jancu et al.¹² In that case, the leading terms come from BIA invariants specific to the L valleys in combination with the L -valley coupling. For Si-Ge (001)-grown QWs the interplay of IIA with X_z valley coupling was examined from the $\mathbf{k} \cdot \mathbf{p}$ theory point of view and semi-quantitative estimates were discussed in the frame of tight-binding calculations based on the sp^3s^* model.¹¹ However, it is well known that this simple model cannot reproduce quantitatively the properties of zone edge valleys such as effective masses and dipole matrix element. This difficulty was solved in the late nineties by the introduction of the extended basis $sp^3d^5s^*$ tight binding model.¹⁶ More recently, progress in the parametrization of this model have led to essentially perfect description of the electronic properties of bulk Ge¹⁷ and Si.¹⁸ In this work, we use the advanced tight-binding model in combination with the envelope function approach and calculate the conduction band spin splitting resulting from the interplay of valley coupling with the IIA and electric-field effects in Si/SiGe quantum wells.

II. POINT-GROUP SYMMETRY ANALYSIS

In the virtual-crystal approximation for SiGe alloys, an ideal (001)-grown SiGe/Si/SiGe QW structure with an odd number N of Si atomic planes has the point-group symmetry D_{2d} which allows the spin-dependent term $\alpha(\sigma_x k_x - \sigma_y k_y)$ in the electron effective Hamiltonian, where σ_x, σ_y are the Pauli spin matrices, \mathbf{k} is the two-dimensional wave vector with the in-plane components k_x, k_y , and $x \parallel [100], y \parallel [010]$. The QW structures with even N have the D_{2h} point symmetry containing the space-inversion center, the constant α is zero and the two-dimensional electronic states are doubly degenerate. Under an electric field $\mathbf{F} = (0, 0, F_z)$ applied along the growth direction z the symmetry of QW structures with both odd and even numbers of Si monoatomic layers reduces to the C_{2v} point group and the spin-dependent linear- \mathbf{k} Hamiltonian becomes

$$\mathcal{H}^{(1)}(\mathbf{k}) = \alpha(\sigma_x k_x - \sigma_y k_y) + \beta(\sigma_x k_y - \sigma_y k_x), \quad (1)$$

where the second contribution is usually called the Rashba term (or the SIA term). In order to establish the parity of α, β with respect to inversion of the electric field we note that, in the D_{2d} group, the combination $h(\mathbf{k}) = \sigma_x k_x - \sigma_y k_y$ as well as even powers of F_z are invariants while both the combination $h'(\mathbf{k}) = \sigma_x k_y - \sigma_y k_x$ and odd powers of F_z transform according to the same representation B_2 (in notations of Ref. 19). Therefore, for structures with odd N , the coefficients α and β are, respectively, even and odd functions of F_z . They can be presented as

$$\begin{aligned} \alpha(F_z; \text{odd } N) &= \alpha_0 + c_\alpha^{(2)} F_z^2 + c_\alpha^{(4)} F_z^4 + \dots, \\ \beta(F_z; \text{odd } N) &= c_\beta^{(1)} F_z + c_\beta^{(3)} F_z^3 + \dots, \end{aligned} \quad (2)$$

where $\alpha_0 \equiv \alpha(0)$ and $c_\alpha^{(2n)}, c_\beta^{(2n+1)}$ are field-independent coefficients. Similarly, for structures with even N , the linear-in- \mathbf{k} spin-dependent Hamiltonian can be presented in the form

$$\mathcal{H}^{(1)}(F_z; \text{even } N) = F_z [C_1 h(\mathbf{k}) + C_2 h'(\mathbf{k})], \quad (3)$$

where C_1, C_2 are even functions of F_z . The above representation follows immediately if we take into account that, with respect to operations of the D_{2h} group, both $h(\mathbf{k})$ and $h'(\mathbf{k})$ transform in the same way as the component F_z does.

The aim of this work is to calculate and analyze the electric field dependencies of α and β . For this purpose we use the precise nearest-neighbor $sp^3d^5s^*$ tight-binding model¹⁶ and calculate valley and spin splittings in symmetrical QWs in the absence and presence of an external electric field.

III. TIGHT-BINDING MODEL

To calculate electron subband splittings, we use the $sp^3d^5s^*$ tight-binding theory elaborated by Jancu et al.¹⁶

It perfectly reproduces band structure of indirect bulk semiconductors as well as electron effective masses, etc. In particular the parametrization used in this work reproduces the value $k_0=85\%$ of the conduction band minimum in Si, which was considered as a challenge.²⁰ One of the main advantages of this method is a very straightforward treatment of nanostructures.

In Ref. 11, we estimated the electron spin splitting in symmetrical SiGe QWs using a less detailed tight-binding model, namely, the sp^3s^* model, which allowed us to understand the main qualitative features of spin splitting as well as to demonstrate the possible observability of this effect in Si/SiGe heterostructures.

In the tight-binding model the electron wave function is written as a linear combination of atomic orbitals²¹

$$|\psi, \mathbf{r}\rangle = \sum_{n,\nu} C_{n,\nu} |\Psi_{\nu}, \mathbf{r} - \mathbf{r}_n\rangle, \quad (4)$$

where n enumerates atoms in the structure, ν runs through the set of spinor orbitals at the n th atom. In the $sp^3d^5s^*$ model, this set includes the orbitals s, p_η ($\eta = x, y, z$), d_ξ ($\xi = yz, xz, yz, x^2 - y^2, 2z^2 - x^2 - y^2$) and s^* multiplied by the spinors \uparrow and \downarrow . We assume the basic orbital functions to be orthogonal. Anyway, this can be achieved using the Löwdin orthogonalization procedure.²² Thus, the tight-binding Hamiltonian is presented as a multicomponent matrix and the Schrödinger equation as an eigenvalue problem

$$\sum_{n',\nu'} \langle \Psi_{n,\nu} | H | \Psi_{n',\nu'} \rangle C_{n',\nu'} = E C_{n,\nu}, \quad (5)$$

where $|\Psi_{n,\nu}\rangle = |\Psi_{\nu}, \mathbf{r} - \mathbf{r}_n\rangle$. The Hamiltonian matrix elements depend on the relative position of atoms, $\mathbf{r}_n - \mathbf{r}_{n'}$, and chemical type of atoms n and n' . We use here the nearest neighbour approximation where the matrix elements differ from zero only for neighbouring atoms. The detailed procedure of constructing the tight-binding Hamiltonian can be found in Ref. 21. Strain effects can be included by scaling the matrix elements with respect to the bond-angle distortions and bond-length changes.²³

For the SiGe alloy we use the virtual crystal approximation (VCA) in order to concentrate on the intrinsic structure symmetry thus neglecting all effects of disorder. Tight-binding parameters were optimized to carefully reproduce alloy band structure. We treat strain in two independent ways: first, atomic positions used in calculations are chosen by using Van de Walle's model.²⁴ We have also applied Keating's Valence Force Field (VFF) model²⁵ with the SiGe parameters from Ref. 26 and found no difference between the continuous and atomistic approaches.

In addition to the strain dependence of tight-binding parameters we have corrected the structure potential (see below) with respect to experimentally observed Si/Si_{1-x}Ge_x conduction-band offset.^{27,28}

We treat an electric field in the tight-binding approach in the following way:²⁹ the diagonal matrix elements of

the tight-binding Hamiltonian are shifted due to the potential of the applied electric field

$$\begin{aligned} \langle \Psi_{n,\nu} | H | \Psi_{n',\nu'} \rangle \\ = \langle \Psi_{n,\nu} | H | \Psi_{n',\nu'} \rangle_{U=0} + U(\mathbf{r}_n) \delta_{nn'} \delta_{\nu\nu'}, \quad (6) \end{aligned}$$

where $U(\mathbf{r})$ is the electric potential energy.

Since we are interested in the in-plane dispersion of free electrons in a heterostructure we impose periodical boundary conditions in the interface plane (001). Because of the periodicity in the [100] and [010] directions we can introduce the in-plane wave vector \mathbf{k} and, for a given value of \mathbf{k} , construct the tight-binding Hamiltonian with a discrete spectrum. For the sake of numerical simplicity we also use periodic boundary conditions along the growth direction [001] taking the barrier layers thick enough to exclude the influence of their thickness on the calculated values of α and β . It follows immediately from the band structure of silicon and SiGe/Si/SiGe structure potential that, neglecting the valley splitting, the electronic states with $k_x = k_y = 0$ are four-fold degenerate. We will focus on the dispersion of the lowest conduction subband $e1$. The interface-induced valley mixing leads to a splitting of the state $|e1, \mathbf{k} = 0\rangle$ into two spin-degenerate states denoted $+$ (upper subband) and $-$ (lower subband). At nonzero \mathbf{k} each subband, $+$ and $-$, undergoes the spin-orbit splitting described by Eq. (1) with the coefficients α_{\pm} and β_{\pm} for the valley-orbit split subbands \pm . It is instructive to rewrite Eq. (1) in the coordinate frame $x' \parallel [1\bar{1}0], y' \parallel [110]$ as follows

$$\mathcal{H}^{(1)}(\mathbf{k}) = (\alpha_{\pm} + \beta_{\pm})\sigma_{x'}k_{y'} + (\alpha_{\pm} - \beta_{\pm})\sigma_{y'}k_{x'}. \quad (7)$$

Let us introduce the energy difference $\Delta_{\text{so}}^{(\pm)}(\mathbf{k} \parallel [1\bar{1}0])$ for the states $|\pm, \mathbf{k} \parallel [1\bar{1}0]\rangle$ with the spin polarized parallel and antiparallel to [110], and $\Delta_{\text{so}}^{(\pm)}(\mathbf{k} \parallel [110])$ for the states $|\pm, \mathbf{k} \parallel [110]\rangle$ with the spin polarized parallel and antiparallel to $[1\bar{1}0]$. The modulus of $\Delta_{\text{so}}^{(\pm)}(\mathbf{k})$ gives the spin splitting of the \pm subbands and the sign of $\Delta_{\text{so}}^{(\pm)}(\mathbf{k})$ determines the relative position of the split spin sublevels. It follows from Eq. (7) and the definition of $\Delta_{\text{so}}^{(\pm)}(\mathbf{k})$ that the constants $\alpha_{\pm}, \beta_{\pm}$ can be found from

$$\begin{aligned} \alpha_{\pm} &= \lim_{k \rightarrow +0} \frac{\Delta_{\text{so}}^{(\pm)}(\mathbf{k} \parallel [110]) + \Delta_{\text{so}}^{(\pm)}(\mathbf{k} \parallel [1\bar{1}0])}{4|\mathbf{k}|}, \quad (8) \\ \beta_{\pm} &= \lim_{k \rightarrow +0} \frac{\Delta_{\text{so}}^{(\pm)}(\mathbf{k} \parallel [110]) - \Delta_{\text{so}}^{(\pm)}(\mathbf{k} \parallel [1\bar{1}0])}{4|\mathbf{k}|}. \end{aligned}$$

Also it should be pointed out that, since the studied QWs are quite shallow, the electron dispersion should be treated with care. To avoid non-linear effects, very small values of k_x, k_y should be considered.

IV. RESULTS AND DISCUSSION

A. Numerical $sp^3d^5s^*$ model calculations: unbiased structure

In order to test and improve our previous results we calculated valley and spin splitting in symmetrical Si QW with $\text{Si}_{0.75}\text{Ge}_{0.25}$ barriers as a function of the QW width. For SiGe composition we used optimized tight-binding parameters precisely reproducing realistic alloy band structure. The strategy for parameterization of the Ge-Si alloy in a virtual crystal approximation is as follows: the parameters of Ge and Si hydrostatically strained to the alloy parameter are first calculated and linearly interpolated. The small remaining differences with measured values are then corrected by fine tuning of a few two-center parameters. For interface atoms we use linear combination of pure Si parameters and alloy.

Tight-binding parameters are optimised for bulk materials. However, band offsets at the interfaces in the heterostructure are also important. For conduction band offset we use Shäffler's paper²⁷ as a reference. Thus, we take a value of 150 meV as a conduction band offset for X_z valley electrons.

Figure 1 shows the zero-field results of calculation of (a) the valley splitting Δ_v and (b) the constants α_{\pm} for the valley split $e1$ subbands in a symmetrical single QW structure with N Si atomic planes sandwiched between the thick $\text{Si}_{0.75}\text{Ge}_{0.25}$ barriers. The splittings as a function of N exhibits oscillations, in agreement with Refs. 10,11,13,15. In Fig. 1 X-shaped crosses depicted as vortices of the broken line represent the calculation in the envelope-function approximation, see below. The broken line is drawn for the eye. Note that, in order to simplify comparison with results obtained by other authors, Fig. 1a illustrates the valley splitting not only for the QW width region $15 \div 50$ Å but also for the region $60 \div 70$ Å.

Results obtained in the framework of the advanced $sp^3d^5s^*$ tight-binding model show considerable difference with our previous estimations.¹¹ The valley splitting is significantly smaller, its value decreases by a factor of 3, whereas the spin splitting increases almost six times. This difference is not unexpected since a careful tight-binding treatment of Si and its compounds is possible in the $sp^3d^5s^*$ model only. In this regard the goal of the previous paper¹¹ was to demonstrate that the effect of spin splitting in macroscopically symmetrical Si quantum wells is measurable and to reveal the main qualitative properties of this splitting.

The previous theoretical values for valley splitting were obtained by both tight-binding^{10,15} and pseudopotential methods.¹³ Although the first two papers utilize the method of calculation similar to that applied here, a straightforward comparison is not possible due to different parametrizations of the $\text{Si}_{1-x}\text{Ge}_x$ alloy, different alloy compositions ($x = 0.2$ in Ref. 10 and 0.3 in Ref. 15) and conduction band offsets used. However, our results are in

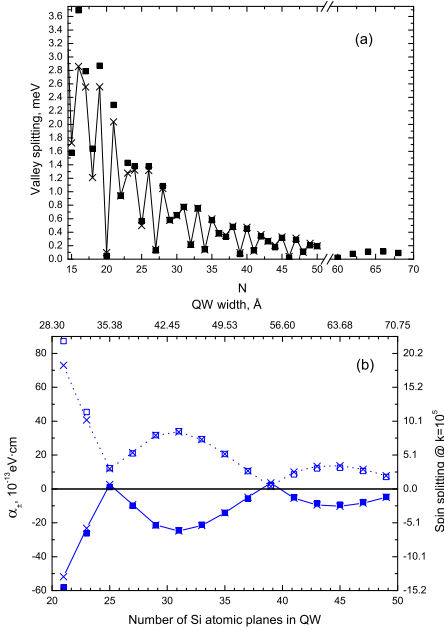


FIG. 1: (a) Valley splitting Δ_v as a function of N in a $\text{Si}_{1-x}\text{Ge}_x/\text{Si}/\text{Si}_{1-x}\text{Ge}_x$ ($x = 0.25$) QW structure in the absence of an electric field. Solid squares and vortices of the broken line represent results of calculations using the tight-binding method and envelope function approximation, respectively. (b) Spin-splitting constants α_{\pm} versus the number N of Si monoatomic layers in the same system (odd N are taken in account only). Spin splitting is shown by solid and open squares ($sp^3d^5s^*$ tight-binding calculation, α_- and α_+ respectively) and x-shaped crosses (envelope function approximation).

good agreement with the both estimations. For example, for a QW containing 64 Si-atomic layers (32 monomolecular layers, 9 nm) we obtain for the valley splitting ~ 0.11 meV, while Refs. 10 and 15 present the coinciding values of ~ 0.2 . Our analysis shows that the valley splitting is quite sensitive to the SiGe alloy parameters. By using the linear combination of Si and Ge tight-binding parameters for the alloy we could reproduce values of the valley splitting obtained by Boykin et al.¹⁰

Comparison with Ref. 13 is more straightforward. Figure 1 in the cited paper shows dependence of the valley splitting on the barrier Ge content for a 16 Si-atomic layer QW calculated by the empirical pseudopotential method. In particular, for the $\text{Si}_{0.75}\text{Ge}_{0.25}/\text{Si}/\text{Si}_{0.75}\text{Ge}_{0.25}$ QW the valley splitting of about 2.5 meV was obtained¹³ while our estimation is 3.7 meV. This is a good agreement taking into account that the two values are obtained in two completely different approaches for quite narrow QWs where interface effects are extremely important.

Figure 2 shows the valley and spin splitting constants as a function of the conduction band offset for QWs with 31, 32, 33, 34 and 64 Si atomic layers. The fifth structure is taken in order to provide comparison with Refs. 10,15. In Fig. 2, in addition to the tight-binding calculations,

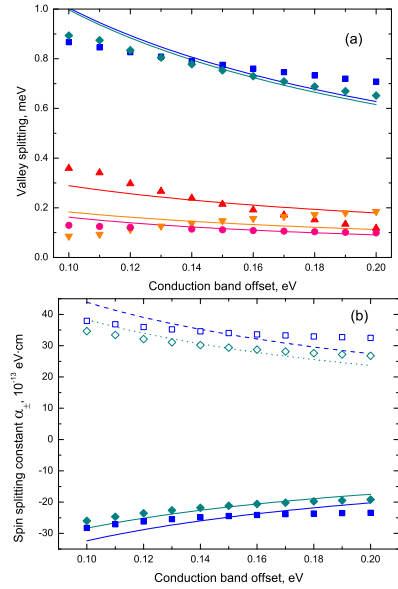


FIG. 2: Valley (a) and spin (b) splittings for the lowest conduction subband versus the conduction band offset. (a) The valley splitting calculated for five QWs with $N = 31$ (■), 32 (▲), 33 (◆), 34 (▼) and 64 (●) Si monoatomic planes. (b) The spin splitting constants α_- (■,◆) and α_+ (□,◇) for 31 (■,□) and 33 (◆,◇) Si atomic layers. The fitting by using the extended envelope function approach is shown by corresponding lines.

we present analytical results on valley and spin splitting in the framework of the extended envelope function approach. A detailed discussion of the analytical treatment is given in subsection IV C. Here we only point out an excellent agreement between results for the splittings as a function of the QW width and satisfactory description of the dependence of these splittings on the band offset.

B. Numerical calculations in the presence of electric field

Figure 3 demonstrates the variation of spin splitting constants with the electric field F_z for the $e1$ valley-split subbands. In accordance with symmetry considerations, the calculations show that the spin splitting becomes anisotropic in QWs with odd numbers of atomic planes and appears in QWs with even numbers of atomic planes. The variation of valley splitting is very weak and we do not present it here.

In order to determine the coefficients α_{\pm} and β_{\pm} we performed the tight-binding calculation of the spin splittings for the electron wave vectors $\mathbf{k} \parallel [110]$ and $\mathbf{k} \parallel [\bar{1}\bar{1}0]$ and then applied Eq. (8) to find the constants α and β directly. The electric field is introduced as a shift of diagonal energies in the tight-binding Hamiltonian. In accordance with Eq. (6), we choose electrostatic potential to be a linear function of z both inside the QW and in the barrier areas near the interfaces. The area of the

constant electric field is extended inside barriers enough to neglect dependence of the splitting on the choice of potential profile. Note that the field values in Fig. 3 are small enough to avoid the tunnelling of an electron from the QW inside the barrier.

At zero electric field, $\beta=0$ for arbitrary value of N and, similarly, $\alpha = 0$ for even N . In this case the spin splitting $\Delta_{\text{so}}(\mathbf{k})$ is independent of the azimuthal angle of the \mathbf{k} vector. However, with increasing the field the diversity in values of α and β for QWs with $N = 31, 32, 33, 34$ decreases.

The further discussion of spin splitting as a function of electric field is continued in the next section. It suffices to note here that within the chosen range of field values, the coefficients α_{\pm} in QWs with odd N are linear functions of F_z^2 . In contrast, in QWs with even numbers of atomic planes where the spin splitting is absent at zero field, α_{\pm} are proportional to F_z . We stress that the field-induced change of α_{\pm} (odd N) becomes comparable to the zero-field value of α_{\pm} in quite weak fields $F_z \sim 4 \cdot 10^4$ V/cm.

In the previous paper¹¹ we developed the extended envelope function model in order to demonstrate that the spin splitting in macroscopically symmetrical QWs is fully defined by interfaces. At non-zero electric field two mechanisms are possible, namely, the SIA and IIA mechanisms. One of the goals of current research is to establish the most important term in realistic QWs. To reveal carefully the comparative role of two mechanisms we present analytical treatment of results shown in Figs. 2 and 3 in the framework of the envelope function approach.

C. Extended envelope function approach

Here we propose an extended envelope function approach¹¹ to describe valley and spin splittings in the presence of an external or built-in electric field. The electron wave function is written as

$$\Psi(\mathbf{r}) = e^{i\mathbf{k}_{\parallel}\cdot\boldsymbol{\rho}}[\varphi_1(z)\psi_{\mathbf{k}_0}(\mathbf{r}) + \varphi_2(z)\psi_{-\mathbf{k}_0}(\mathbf{r})], \quad (9)$$

where $\psi_{\pm\mathbf{k}_0}(\mathbf{r}) = e^{\pm i\mathbf{k}_0\cdot\mathbf{r}}u_{\pm\mathbf{k}_0}(\mathbf{r})$ is the Bloch function at the the extremum points $\pm\mathbf{k}_0$ on the line Δ in the Brillouin zone. The spinor envelopes φ_1, φ_2 in Eq. (9) are conveniently presented as a four-component bispinor

$$\hat{\varphi}(z) = \begin{bmatrix} \varphi_1(z) \\ \varphi_2(z) \end{bmatrix}. \quad (10)$$

The effective Hamiltonian acting on $\hat{\varphi}(z)$ is written as a 4×4 matrix consisting of the standard zero-approximation Hamiltonian

$$\mathcal{H}_0 = \frac{\hbar^2}{2} \left[-\frac{d}{dz} \frac{1}{m_l(z)} \frac{d}{dz} + \frac{k_x^2 + k_y^2}{m_t(z)} + U(z) \right] \quad (11)$$

which is independent of valley and spin indices, and an interface-induced δ -functional perturbation

$$\mathcal{H}' = \hat{V}_L \delta(z - z_L) + \hat{V}_R \delta(z - z_R). \quad (12)$$

Here m_l and m_t are the longitudinal and transverse electron effective mass in the Δ valley of the bulk material, z_L and z_R are the coordinates of the left- and right-hand-side interfaces, the potential energy $U(z)$ is referred to the bottom of the conduction band in Si and given by

$$U(z) = V\theta_b(z) - eF_z z$$

with V being the conduction-band offset, $\theta_b(z) = 1$ in the SiGe barrier layers and $\theta_b(z) = 0$ inside the Si layer. The explicit form of the matrices $\hat{V}_{L,R}$ obtained by using symmetry considerations is presented in Ref. 11.

In the zero approximation, i.e., neglecting the valley-orbit and spin-orbit coupling, $\hat{V}_{L,R} = 0$, the bispinor is given by

$$\hat{\varphi}(z) = \begin{bmatrix} c_1 \\ c_2 \end{bmatrix} \chi(z),$$

where c_1, c_2 are arbitrary z -independent spinors and the function $\chi(z)$ satisfies the Schrödinger equation

$$\mathcal{H}_0 \chi(z) = E \chi(z). \quad (13)$$

In the following we take into consideration only the lowest size-quantized electronic subband $e1$.

The next step is an allowance for the interface-induced spin-independent mixing between the valleys \mathbf{k}_0 and $-\mathbf{k}_0$ described by the matrices

$$\hat{V}_R = \begin{bmatrix} 0 & \Lambda_R \\ \Lambda_R^* & 0 \end{bmatrix}, \quad \hat{V}_L = \begin{bmatrix} 0 & \Lambda_L \\ \Lambda_L^* & 0 \end{bmatrix},$$

where $\Lambda_R = \lambda e^{-ik_0 a}$, $\Lambda_L = \lambda e^{ik_0 a}$, $a = z_R - z_L = Na_0/4$ is the QW width, a_0 is the microscopic lattice constant, and λ is a complex coefficient.

In terms of the envelope $\chi(z)$ the matrix element of valley mixing can be written as

$$\langle 1|\mathcal{H}'|2\rangle = |\lambda| [(\chi_L^2 + \chi_R^2) \cos(k_0 a - \phi_\lambda) + i(\chi_L^2 - \chi_R^2) \sin(k_0 a - \phi_\lambda)], \quad (14)$$

where $|\lambda|$ and ϕ_λ are the modulus and the phase of λ , $\chi_{R,L}$ are the values of the envelope χ at the right and left interfaces, $\chi(\pm a/2)$, respectively. The valley-orbit split states have the energy $E_{\pm} = E_0 \pm |\langle 1|\mathcal{H}'|2\rangle|$, where E_0 is the eigen energy of Eq. (13), so that the splitting is equal to

$$\Delta_v = 2|\langle 1|\mathcal{H}'|2\rangle| = 2|\lambda| \sqrt{\chi_L^4 + \chi_R^4 + 2\chi_L^2 \chi_R^2 \cos[2(k_0 a - \phi_\lambda)]}. \quad (15)$$

The bispinors for the upper (+) and lower (-) states are given by

$$\hat{\varphi}_{\pm,s}(z) = \frac{1}{\sqrt{2}} \begin{bmatrix} c_s \\ \pm e^{-i\phi_M} c_s \end{bmatrix}, \quad (16)$$

where c_s is spinor \uparrow for the electron spin $s = 1/2$ and \downarrow for the electron spin $s = -1/2$, ϕ_M is the phase of the matrix element (14).

The tight-binding calculations show that the spin splitting is much smaller as compared to the valley splitting Δ_v . Therefore, the spin splitting can be considered independently for the upper and lower valley-orbit split states (16). The corresponding matrix elements are reduced to

$$\mathcal{H}'_{ss'}(\mathbf{k}; e1, \pm) = M_{1s,1s'} \pm \left(\text{Re}\{M_{1s,2s'}\} \cos \phi_M + \text{Im}\{M_{1s,2s'}\} \sin \phi_M \right), \quad (17)$$

where the subscript indices 1, 2 enumerate the valleys $\mathbf{k}_0, -\mathbf{k}_0$ and $s, s' = \pm 1/2$ are the spin indices, the components $M_{1s,1s'}, M_{1s,2s'}$ written as 2×2 matrices M_{11}, M_{12} are related to similar 2×2 matrices $V_{R,11}, V_{L,11}, V_{R,12}, V_{L,12}$ by

$$M_{11} = \chi_L^2 V_{L,11} + \chi_R^2 V_{R,11}, \quad M_{12} = \chi_L^2 V_{L,12} + \chi_R^2 V_{R,12}.$$

The spin-dependent contributions to $V_{R,11}, V_{L,11}, V_{R,12}, V_{L,12}$ are linear combinations of $h(\mathbf{k})$ and $h'(\mathbf{k})$, see Ref. 11:

$$\hat{V}_R = \begin{bmatrix} S h(\mathbf{k}) + S' h'(\mathbf{k}) & [\lambda + p h(\mathbf{k}) + p' h'(\mathbf{k})] e^{-ik_0 a} \\ [\lambda^* + p^* h(\mathbf{k}) + p'^* h'(\mathbf{k})] e^{ik_0 a} & S h(\mathbf{k}) + S' h'(\mathbf{k}) \end{bmatrix} \quad (18)$$

and similar equation for \hat{V}_L with the coefficients interrelated with λ, S, S', p, p' due to the mirror-rotation operation \mathcal{S}_4 (odd N) or the inversion i (even N) which transforms the right-hand-side interface into the left-hand-side one. Taking into account the relation between coefficients entering the matrices \hat{V}_R and \hat{V}_L and the notations of Ref. 11 we can write the spin Hamiltonians (17) in the form of Eq. (1), namely,

$$\mathcal{H}^{(1)}(\mathbf{k}; e1, \pm) = \alpha_{\pm} h(\mathbf{k}) + \beta_{\pm} h'(\mathbf{k}). \quad (19)$$

For the coefficients $\alpha_{\pm}, \beta_{\pm}$ describing the spin splitting of the valley-orbit split subbands, we obtain

$$\alpha_{\pm} = [\chi_R^2 - (-1)^N \chi_L^2] S \pm |p| H_{\alpha}(\phi_p), \quad (20)$$

$$\beta_{\pm} = (\chi_R^2 - \chi_L^2) S' \mp |p'| H_{\beta}(\phi_{p'}).$$

Here

$$H_{\alpha}(\phi) = \chi_R^2 \cos(k_0 a - \phi + \Phi) - (-1)^N \chi_L^2 \cos(k_0 a - \phi - \Phi)$$

$$H_{\beta}(\phi) = \chi_R^2 \cos(k_0 a - \phi + \Phi) - \chi_L^2 \cos(k_0 a - \phi - \Phi),$$

$$\Phi = \arg \left(\chi_L^2 e^{i(k_0 a - \phi_{\lambda})} + \chi_R^2 e^{-i(k_0 a - \phi_{\lambda})} \right),$$

the parameters S, S' describe the intra-valley contributions to the interface-induced electron spin mixing, and the parameters $p = |p| e^{i\phi_p}, p' = |p'| e^{i\phi_{p'}}$ describe the spin-dependent inter-valley mixing. Oscillatory dependence of the valley and spin splittings on the QW thickness a is caused by interference of electron waves arising from inter-valley reflection off the left- and right-hand side interfaces.

D. Comparison between tight-binding and envelope function approach

In the absence of an electric field, one has $\chi_L^2 = \chi_R^2$, $\Phi = 0$ for positive and $\Phi = \pi$ for negative values of $\cos(k_0 a - \phi_{\lambda})$, and Eqs. (15), (20) reduce to¹¹

$$\Delta_v = 4\chi_L^2 |\lambda \cos(k_0 a - \phi_{\lambda})|,$$

$\alpha_{\pm} = \beta_{\pm} = 0$ for even N , and

$$\alpha_{\pm} = 2\chi_L^2 [S \pm \eta |p| \cos(k_0 a - \phi_p)], \quad \beta_{\pm} = 0$$

for odd N , where $\eta = e^{i\Phi} = \text{sign}\{\cos(k_0 a - \phi_{\lambda})\}$. The curves in Fig. 1 are calculated by using the following best-fit set of parameters: $|\lambda| = 65 \text{ meV} \cdot \text{\AA}$, $\phi_{\lambda} = 0.013\pi$, $|p| = 4450 \text{ meV} \cdot \text{\AA}^2$, $\phi_p = 0.095\pi$, $S = 650 \text{ meV} \cdot \text{\AA}^2$.

Although tight-binding-model values of the coefficients in the present work are quite different from the previous estimations, the envelope function approach proves its adequate description of the valley and spin splittings as a function of the QW width. The analytical approach with merely five parameters perfectly fits the complex microscopical calculation.

Comparison of new results with experimental data of Wilamovsky et al.³⁰ shows the better agreement. With the necessary correction³¹ the experimental results give $\sim 0.34 \times 10^{-12} \text{ eV} \cdot \text{\AA}$ for the spin splitting constant in a 120\text{\AA}-thick QW. The more detailed comparison should be done with caution since effects of disorder and built-in electric fields can have crucial influence. However, the coincidence in an order of magnitude shows that our calculations agree with the available experimental data.

According to Fig. 2, the description of dependence of spin splitting on the band offset is not so perfect in the framework of envelope function approach. In fact, the variation in band offset results in a complex (obviously

non-linear) behaviour of the parameters in the boundary conditions at the interfaces.

Figure 3 is the main result of this work and we discuss it in more details. The agreement between the two approaches seen in Fig. 3a shows that the extended envelope function approach catches the physics of spin splitting induced by the applied electric field. Moreover, the fact that this agreement takes place with no addition of a SIA term shows that in the system under study the IIA contribution is dominating. It should be noted that Eq. (20) for α_{\pm} contains only parameters which can be extracted from Fig. 1, and, indeed, Fig. 3a does not contain any fitting parameters. Additional fitting parameters used to describe Fig. 3b are as follows: $|p'| = 700 \text{ meV}\cdot\text{\AA}^2$, $\phi_{p'} = \pi$ and $S' = 70 \text{ meV}\cdot\text{\AA}^2$.

In the high-field limit $\chi_L\chi_R/(\chi_L^2 + \chi_R^2) \rightarrow 0$ so that either $\chi_L^2 \ll \chi_R^2$ or $\chi_L^2 \gg \chi_R^2$, and Eqs. (15), (20) transfer to

$$\Delta_v = 2|\lambda| \max\{\chi_L^2, \chi_R^2\},$$

$$\alpha_{\pm} = 2 \text{sign}\{F_z^{N+1}\} [S \pm |p| \cos(\phi_p - \phi_{\lambda})] \max\{\chi_L^2, \chi_R^2\},$$

$$\beta_{\pm} = 2 \text{sign}\{F_z\} [-S' \mp |p'| \cos(\phi_{p'} - \phi_{\lambda})] \max\{\chi_L^2, \chi_R^2\}.$$

Since one of the interfaces becomes inaccessible to the electron the oscillatory behavior vanishes in strong fields.

It should be stressed that the parity of the coefficients α_{\pm} and β_{\pm} following from the above equations completely agrees with the general symmetry considerations, see Eqs. (2) and (3). We also note that a monoatomic shift as a whole of the QW position in the structure results in an inversion of sign of α_{\pm} while the values of β_{\pm} remain unchanged.

V. CONCLUSION

The $sp^3d^5s^*$ tight-binding model has been used to calculate the electron dispersion in heterostructures grown from multivalley semiconductors with the diamond lattice, particularly, in the Si/SiGe structures. The model allows one to estimate quantitatively the valley and spin splittings of electron states in the quantum-confined ground subband as well as the electric-field dependence of the spin splitting. In the employed tight-binding model, this splitting is mostly determined by the spin-dependent mixing at the interfaces. As a result the coefficients describing the Dresselhaus term in unbiased QWs are oscillating functions of the odd number N of Si monoatomic layers. Under an electric field applied along the growth axis a non-zero Rashba term appears in QWs with both even and odd Si atomic layers. In small fields, the Dresselhaus term is linear in the structures with even N (D_{2h} point group) and quadratic in structures with odd N (D_{2d} point group). Thus, in quite low fields about $10^{-4} \text{ eV}\cdot\text{cm}$ the spin splitting becomes anisotropic and oscillations as a function of the QW width are suppressed.

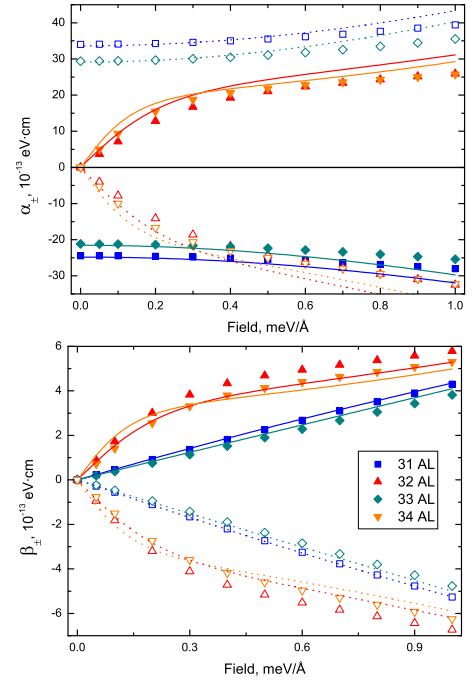


FIG. 3: Spin-splitting constants α_{\pm} and β_{\pm} for the lowest conduction subband versus the electric field F_z calculated for four QWs with 31, 32, 33 and 34 Si monoatomic planes. Points are calculated in the $sp^3d^5s^*$ tight-binding model. Lines represent fitting by using the extended envelope function approach.

In addition to numerical calculations, an extended envelope function approach is utilized to interpret the results of tight-binding calculations. The inclusion of spin-dependent reflection of an electronic wave at the interface and interface-induced inter-valley mixing permits one to describe quite well the numerical dependencies of the valley-orbit and spin-orbit splittings upon the number of Si atomic planes and the electric field.

Acknowledgments

This work was financially supported by RFBR and CNRS PICS projects, programmes of RAS and “Dynasty” Foundation — ICFPM.

-
- ¹ E. I. Rashba, Fiz. Tverd. Tela **2**, 1224 (1960), [Sov. Phys. Solid State **2**, 1109 (1960)].
 - ² Y. A. Bychkov and E. I. Rashba, Pis'ma Zh. Eksp. Teor. Fiz. **9**, 66 (1984), [JETP Lett. **39**,78 (1984)].
 - ³ L. Vervoort, R. Ferreira, and P. Voisin, Phys. Rev. B **56**, R12744 (1997).
 - ⁴ L. Vervoort, R. Ferreira, and P. Voisin, Semicond. Science and Technology **14**, 227 (1999).
 - ⁵ E. L. Ivchenko, A. Y. Kaminski, and U. Rössler, Phys. Rev. B **54**, 5852 (1996).
 - ⁶ T. Guettler, A. L. C. Triques, L. Vervoort, R. Ferreira, P. Roussignol, P. Voisin, D. Rondi, and J. C. Harmand, Phys. Rev. B **58**, 10179 (1998).
 - ⁷ J. T. Olesberg, W. H. Lau, M. E. Flatté, C. Yu, E. Altunkaya, E. M. Shaw, T. C. Hasenberg, and T. F. Boggess, Phys. Rev. B **64**, 201301 (2001).
 - ⁸ K. C. Hall, K. Gündoğdu, E. Altunkaya, W. H. Lau, M. E. Flatté, T. F. Boggess, J. J. Zinck, W. B. Barvosa-Carter, and S. L. Skeith, Phys. Rev. B **68**, 115311 (2003).
 - ⁹ L. E. Golub and E. L. Ivchenko, Phys. Rev. B **69**, 115333 (2004).
 - ¹⁰ T. B. Boykin, G. Klimeck, M. Friesen, S. N. Coppersmith, P. von Allmen, F. Oyafuso, and S. Lee, Phys. Rev. B **70**, 165325 (2004).
 - ¹¹ M. O. Nestoklon, L. E. Golub, and E. L. Ivchenko, Phys. Rev. B **73**, 235334 (2006).
 - ¹² J.-M. Jancu, R. Scholz, E. A. de Andrada e Silva, and G. C. L. Rocca, Phys. Rev. B **72**, 193201 (2005).
 - ¹³ A. Valavanis, Z. Ikonic, and R. W. Kelsall, Phys. Rev. B **75**, 205332 (2007).
 - ¹⁴ M. Virgilio and G. Grosso, Phys. Rev. B **75**, 235428 (2007).
 - ¹⁵ M. Friesen, S. Chutia, C. Tahan, and S. N. Coppersmith, Phys. Rev. B **75**, 115318 (2007).
 - ¹⁶ J.-M. Jancu, R. Scholz, F. Beltram, and F. Bassani, Phys. Rev. B **57**, 6493 (1998).
 - ¹⁷ J.-M. Jancu and P. Voisin, Phys. Rev. B **76**, 115202 (2007).
 - ¹⁸ F. Sacconi, A. Di Carlo, P. Luigli, M. Städele, and J.-M. Jancu, IEEE Transactions on Electron Devices **51**, 704 (2004).
 - ¹⁹ G. Bir and G. Pikus, *Symmetry and Strain Induced Effects in Semiconductors* (Wiley, New York, 1974).
 - ²⁰ G. Klimeck, R. C. Bowen, T. B. Boykin, C. Salazar-Lazaro, T. A. Cwik, and A. Stoica, Superlattices and Microstructures **27**, 77 (2000).
 - ²¹ J. C. Slater and G. F. Koster, Phys. Rev. **94**, 1498 (1954).
 - ²² P.-O. Löwdin, The Journal of Chemical Physics **18**, 365 (1950).
 - ²³ S. Y. Ren, J. D. Dow, and D. J. Wolford, Phys. Rev. B **25**, 7661 (1982).
 - ²⁴ C. G. Van de Walle, Phys. Rev. B **39**, 1871 (1989).
 - ²⁵ P. N. Keating, Phys. Rev. **145**, 637 (1966).
 - ²⁶ J. E. Bernard and A. Zunger, Phys. Rev. B **44**, 1663 (1991).
 - ²⁷ F. Schäffler, Semicond. Sci. Technol. **12**, 1515 (1997).
 - ²⁸ M. M. Rieger and P. Vogl, Phys. Rev. B **48**, 14276 (1993).
 - ²⁹ T. B. Boykin and P. Vogl, Phys. Rev. B **65**, 035202 (2001).
 - ³⁰ Z. Wilamowski, W. Jantsch, H. Malissa, and U. Rössler, Phys. Rev. B **66**, 195315 (2002).
 - ³¹ M. M. Glazov, Phys. Rev. B **70**, 195314 (2004).